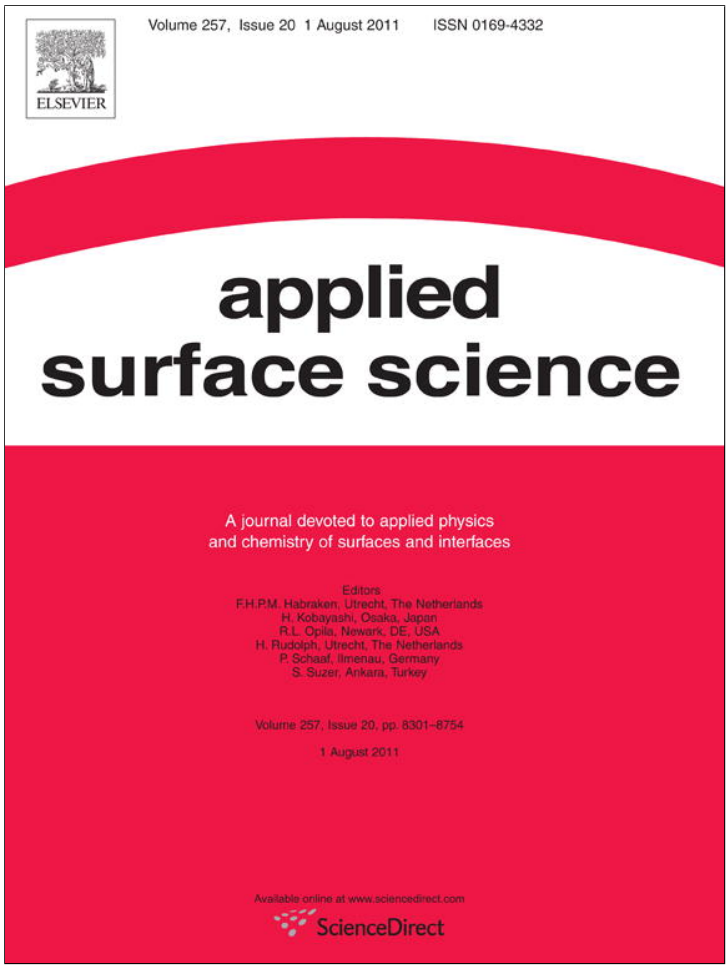

Applied Surface Science 257 (2011) 8409–8412

Contents lists available at ScienceDirect

Applied Surface Science

journal homepage: www.elsevier.com/locate/apsusc

Tuning photoresponse through size distribution control of silicon quantum dots

C. Xu, Z.P. Li, W. Pan, W.Z. Shen*

Laboratory of Condensed Matter Spectroscopy and Opto-Electronic Physics, and Key Laboratory of Artificial Structures and Quantum Control (Ministry of Education), Department of Physics, Shanghai Jiao Tong University, 800 Dong Chuan Road, Shanghai 200240, China

ARTICLE INFO

Article history:
Received 24 September 2010
Received in revised form 20 April 2011
Accepted 21 April 2011
Available online 28 April 2011

Keywords:
Photoresponse
Size distribution
Quantum dots
Silicon

ABSTRACT

We report a detailed experimental and theoretical investigation on the photocurrent characteristics of nanocrystalline Si thin films, with the emphasis on the effect of Si dot size distribution. Broader photocurrent response has been observed in Si quantum dots with larger size dispersion due to the improvement of light harvest. As a result of tunneling loss in the expanded energy distribution, we have demonstrated that there is a tradeoff between the absorption enhancement and reduced transport for the photocurrent intensity. The present work opens new strategy to maximize the photoresponse through size distribution control for quantum dot solar cell application.

The emergence of semiconductor nanocrystals as the building blocks of nanotechnology has opened up new ways in next generation solar cells. Nanocrystalline Si (nc-Si) thin film, a mixed-phase material consisting of Si quantum dots embedded in amorphous tissue, presents very promising features [1] in solving the unavoidable disadvantages of low energy conversion efficiency [2] and light-induced degradation [3] of commercial amorphous Si thin film solar cells. Size quantization effect allows one to tune the photoresponse easily, making nc-Si thin film a good light harvester. Strong optical absorption and high photocurrent have been found in nc-Si films and attributed to the enhancement of the optical absorption cross section and good carrier conductivity in the nanometer grains [4]. There are a number of attempts to realize high efficiency and good stability single-junction [5] and tandem [1,6] third generation nc-Si thin film solar cells, ready to make a substantial contribution to the world's photovoltaic market.

While modulation of band energies through size quantization effect offers a good way to control the photoresponse and photoconversion efficiency of quantum dot solar cells, we present in this paper a novel strategy to maximize the photoresponse through size distribution control of the Si quantum dots. In most quantum dot based optoelectronic devices, it is imperative to achieve good dot size uniformity because the size variation gives rise to an inhomogeneous broadening of optical transitions resulting from carrier recombination or generation. However, the inherent size distribution in quantum dot structures can provide a marked improvement of light harvest for the potential application in quantum dot rainbow solar cells [7,8] to boost the energy conversion limit. Although expanded energy distribution sacrifices the transport characteristics of the photogenerated carriers, broad size dispersion will provide instinctive spread in photoresponse spectra. In our previous work [9], we demonstrated that the standard deviation of Si grain sizes could be well characterized by Raman mapping technique and the film uniformity versus doping concentration was correlated in terms of the growth mechanism. Here, we will show that there is a tradeoff between the absorption enhancement and tunneling loss for the photocurrent intensity in Si quantum dots, where a new approach is developed for maximizing light energy conversion with relatively simple and low cost manufacturing process.

The studied nc-Si thin films with thicknesses of ~3 μm were grown on lightly p-doped crystalline Si (1 1 1) substrates (with the resistivity around 10^1–10^2 Ω cm) at a temperature of 250 °C by radio frequency (13.56 MHz) plasma enhanced chemical vapor deposition. The percentage content of phosphine dopant gas (PH_3/SiH_4) C_P ranged from 0 to 20%, while the hydrogen dilution ratio [$H_2/(SiH_4+H_2)$] was kept constant at 99%. The film structure, average dot size, and size distribution have been characterized by room-temperature unpolarized micro-Raman mapping via a Jobin Yvon LabRam HR800UV spectrometer in backscattering configuration under an exciting wavelength of 514.5 nm. The photocurrent measurements were performed on a Nicolet Nexus 870 Fourier transform infrared spectrometer corrected by a DTGS TEC detector. Two indium electrodes were formed on both sides of the nc-Si(n)/c-Si(p) heterostructures, and a variable dc bias was applied through a Keithley 2400 sourcemeter, where temperature-dependent current–voltage measurements were also conducted in an Janis cryostat system.

* Corresponding author.
E-mail address: wzshen@sjtu.edu.cn (W.Z. Shen).

0169-4332/$ – see front matter © 2011 Elsevier B.V. All rights reserved.
doi:10.1016/j.apsusc.2011.04.092

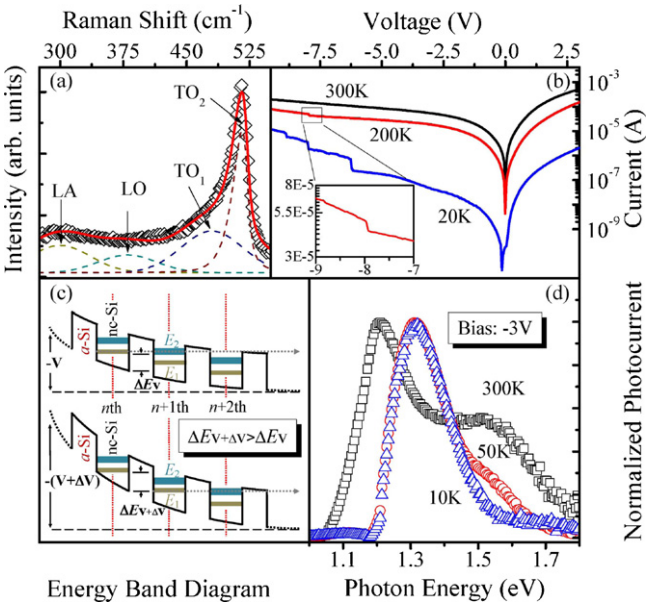

Fig. 1. Optical, electrical, and optoelectronic properties of intrinsic nc-Si thin film (C_P = 0%). (a) Experimental (scatters) and fitted (curves) Raman spectrum. (b) Temperature-dependent current–voltage characteristics with the enlarged staircases at 200 K shown in the inset. (c) Energy diagram at different applied biases. (d) Temperature-dependent normalized photocurrent spectra at a reverse bias of −3 V; spectra are normalized to the same height, taken equal to unity.

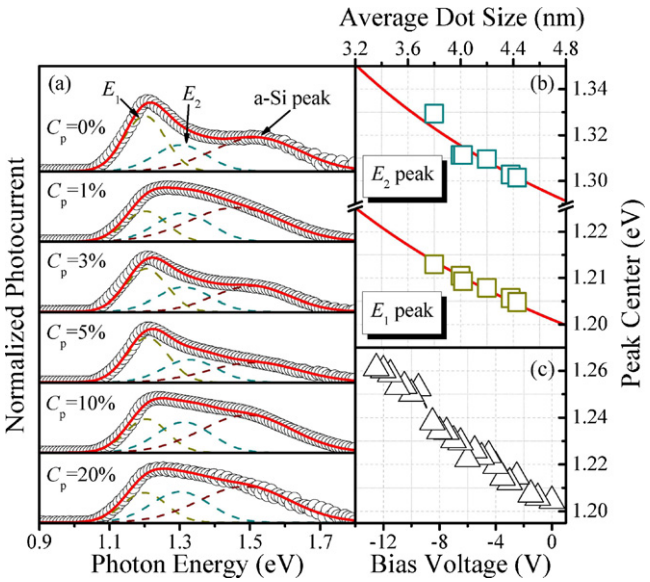

Fig. 2. Experimental (scatters) and fitted (curves) (a) photocurrent spectra for nc-Si thin films with different phosphorus doping concentrations C_P = 0–20%, (b) peak positions of the E_1- and E_2-related transitions with different dot sizes. (c) Shift of photocurrent peak in the intrinsic sample (C_P = 0%) from 1.21 to 1.26 eV with the reverse bias voltage changed from 0 to −12 V.

We start from the optical, electrical, and optoelectronic properties of the nc-Si thin films. Fig. 1(a) presents the decomposed average spectrum of total 100 experimental Raman mapping spectra of the intrinsic sample (C_P = 0%) at 300 K, which clearly exhibits the asymmetric Lorentz shaped transverse optical (TO_2) band peak at ∼520.5 cm^{-1} related to the nanocrystalline silicon and three Gaussian phonon bands with peaks at 300 cm^{-1} [longitudinal acoustic (LA)], 380 cm^{-1} [longitudinal optical (LO)], and 480 cm^{-1} [transverse optical (TO_1)] from the contribution of amorphous silicon. A crystallinity of 54.8% and an average grain size d of 4.4 nm have been deduced from the three-dimensional phonon confinement model [10]. Fig. 1(b) shows the temperature-dependent (20–300 K) current–voltage curves, in which obvious current staircases appear in the bias range from −6 to −9 V at $T \leq 200$ K. The enlarged plot in Fig. 1(b) illustrates a clear current region, which is a characteristic of the Coulomb blockade structure, demonstrating the high order of Si quantum dots and electron tunneling behavior in nc-Si thin films.

It is convenient to explain the staircases by the energy band diagram of nc-Si thin films. As shown in Fig. 1(c), once the ground-state E_1 in nth Si quantum dots, lifted by the applied reverse bias, aligns with the excited-state E_2 in $n+1$th Si nanocrystals, resonant tunneling occurs and the current increases steeply [see Fig. 1(b)]. Before the ground-state in $n+1$th Si quantum dots aligns with the excited-state in $n+2$th Si nanocrystals, tunneling current rises slightly with the increase of reverse bias due to the Coulomb effect, and therefore a flat current region forms. It is the existence of ground- and excited-states in the Si quantum dots that leads to the appearance of the Coulomb staircases in the observed current–voltage characteristics.

Fig. 1(d) displays the normalized photocurrent spectra of the intrinsic sample at a reverse bias of −3 V and temperatures of 300, 50, and 10 K. It is clear that two peaks (at ∼1.2 eV and ∼1.5 eV) can be observed at 300 K. With the decrease of temperature, the low-energy peak that is related to the contribution of photoexcited transition in Si nanocrystals is blueshifted. This phenomenon originates from the effect of dilation of lattice and electron-lattice interaction in quantum dots [11]. In contrast, the high-energy peak position changes little, accompanied with its intensity decreased. This peak mainly comes from the contribution of bandtail transition of amorphous silicon with thermally activated hopping behavior, which is frozen with the decrease of temperature and results in the quenching of the peak below 50 K [12].

Fig. 2(a) shows the room-temperature photocurrent spectra of the nc-Si thin films doped at different percentage contents of phosphine C_P. In contrast to the fact that all the six curves exhibit slowly slide-down shoulder in the high energy region (>1.4 eV) due to the bandtail absorption of the amorphous silicon, we can observe obvious distinction in the broadening of photocurrent peaks at ∼1.2 eV. Since the photocurrent peaks at ∼1.2 eV originate from the contribution of photoexcited transition in Si quantum dots, this variation reflects the effect of the size distribution of Si nanocrystals on the photocurrent response. On the basis of the existence of multiple energy states identified from the current-voltage characteristics in Fig. 1(b), we can decompose [see Fig. 2(a)] the photocurrent spectra into three Gaussian-shaped peaks, which are related to the ground- (E_1) and excited-state (E_2) of Si nanocrystals, as well as the amorphous silicon indicated in the figure. The background photocurrent from the c-Si substrate is negligible for experiencing an absorption by thick nc-Si films (∼3 μm in thickness), and has been subtracted via the method described elsewhere [12].

We plot in Fig. 2(b) the extracted peak positions of E_1- and E_2-related transitions as a function of average grain size d deduced from Raman spectra. It is clear that with the decrease of grain size d, the two peak positions shift toward high energy side, which reflects the quantum confinement effect in Si quantum dots. We can easily find out the relationship between the transition energies and grain sizes [13] with the formula of $1.114 + 0.233d^{-0.674}$ (E_1 transition) and $1.150 + 0.549d^{-0.867}$ (E_2 transition), as shown the solid curves in Fig. 2(b). The relatively weaker confinement with the parameter of ∼−0.674 for the ground-state transition, as compared with the reported result of −0.89 in Si/SiO_2 quantum dot system [14], is reasonable due to the lower confining potential (∼0.4 eV) of our amorphous silicon tissue, showing the penetration of wavefunction into barriers [13]. Further evidence of the assignment on the photocurrent peaks at ∼1.2 eV to the optical absorption in the ground-

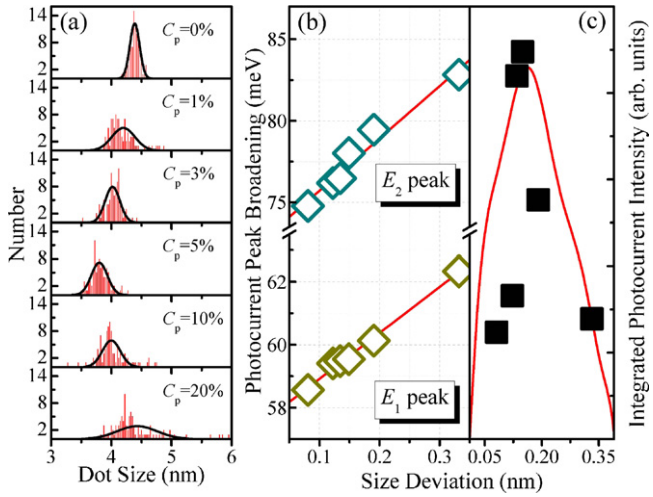

Fig. 3. (a) Experimental histogram of the grain size d from Raman mapping, together with the fitted normal distribution (curves). Experimental (scatters) and calculated (curves) (b) photocurrent peak broadening of the E_1- and E_2-related transitions, (c) integrated photocurrent intensity with different size deviations.

and excited-states in Si nanocrystals comes from the blueshift of the peak position from 1.21 to 1.26 eV with the reverse bias increasing from 0 to −13 V [see Fig. 2(c)], which can be interpreted by the lift of the discrete states in Si nanocrystals as a result of energy band bending, as illustrated in Fig. 1(c).

We now focus on the effect of the size distribution of Si nanocrystals on the E_1- and E_2-related photocurrent response, which will play a key role in the application of nc-Si thin film solar cells. Fig. 3(a) displays the grain size distribution of the six samples from the Raman mapping spectra, together with the normal distribution function fitted at the peak position of the average grain size d. The intrinsic sample (C_p = 0%) has the least dots size deviation of 0.081 nm, exhibiting the narrowest linewidth in the profile, while in doped samples, the dots size deviation firstly drops and then rises with increasing doping concentration. This phenomenon has been interpreted well in Ref. [9]. The introduction of dopant phosphor causes the lattice distortion and results in these microcosmic disorder and macroscopical nonuniformity in nc-Si thin films. The coaction of the two different mechanisms determines the size dispersion of Si nanocrystals in thin films.

Fig. 3(b) presents the photocurrent peak broadening as a function of the grain size deviation. It is clear that both the E_1- and E_2-related photocurrent peak linewidths increase monotonously with the size distribution. Theoretical linear relationship between the size deviation and broadening of optical absorption spectra has been deduced in quantum dot systems [15,16], based on the assumption of infinite potential barriers. Here, we introduce a semi-empirical equation of photoexcited transition in quantum dots, and obtain a more general relationship between the dot size deviation and photoresponse broadening, as will be discussed below.

We propose to use the phenomenological relation $\hbar\omega = E_g + A(n)/R^w$ to represent the photon energy needed for the creation of an electron–hole pair in quantum dots with radius R [13], where E_g is the bandgap of bulk material, $A(n)$ is related to the nth transition in discrete levels, and w is the confinement parameter. The optical absorption coefficient α_s of a single spherical quantum dot with radius R in nth discrete level can be calculated from [17]:

$$\alpha_s = \frac{B}{4/3\pi R^3} g(n)\delta\left[\hbar\omega - \left(E_g + \frac{A(n)}{R^w}\right)\right] \quad (1)$$

where B is a constant related to the momentum matrix element in photoexcited transition and $g(n)$ is the degeneracy of energy level. Considering the normal distribution of dot size $P(R)$ with a standard deviation D_R and an average radius $\bar{R}$, the optical absorption in the system can be expressed as:

$$\alpha = \int_0^\infty P(R)\alpha_s dR = \frac{3B}{\sqrt{32\pi}} \frac{g(n)\bar{R}^{w-2}}{A(n)w} x^{(4/w)-2} \times \exp\left(-\frac{\bar{R}^2}{2D_R^2}\left(\frac{1}{x^{2/w}} - 1\right)^2\right), \quad (2)$$

with one dimensionless parameter $x^2 = \hbar\omega - E_g/A(n)/\bar{R}^w$. The Gaussian peak position is at $x = 1$ with the photon energy $\hbar\omega_{peak} = E_g + A(n)/\bar{R}^w$. In our samples the relative deviation $D_R/\bar{R}$ is very small (<0.08), and the photon energy at $e^{1/2}$ of the maximal absorption is very close to the peak position. We can therefore approximate the broadening of the nth transition peak P_B as:

$$P_B \sim w\frac{A(n)}{\bar{R}^{w+1}} D_R = \frac{w}{\bar{R}}\left(\hbar\omega_{peak} - E_g\right) D_R \quad (3)$$

The solid lines in Fig. 3(b) are the calculated results with the obtained data [$A(n)$ and w] from Fig. 2(b). It is obvious that Eq. (3) can well describe the relationship between the grain size deviation and the photocurrent response broadening, with a slope of 0.015 for the E_1 peak and that of 0.032 for the E_2 peak. The obtained slope of the E_2 peak is about two times larger than that of the E_1 peak, indicating that the photoresponse broadening plays a more notable role in the higher than lower state transition. Moreover, the slope $\frac{w}{\bar{R}}\left(\hbar\omega_{peak} - E_g\right)$ in Eq. (3) shows that quantum dot systems with stronger confinement effect (larger index w and higher confinement energy $\hbar\omega_{peak} - E_g$) will cause a wider span of energy level distribution than those with weaker confinement effect under the same grain size deviation and average grain size. Therefore, broader linewidth of photocurrent response will be observed in quantum dot systems with larger size dispersion and/or stronger quantum confinement effect.

Although spread absorption is very helpful for the improvement of solar cell efficiency, the expanded energy distribution will sacrifice the transport characteristics of the photogenerated carriers. The tunneling coefficient (T_{QD}) is highly sensitive to the position of energy states and its alignment between each other in quantum dot systems. Fig. 3(c) shows the relation of the integrated photocurrent intensity with the size deviation of our samples (scatters). It is clear that there is a tradeoff between the absorption enhancement and tunneling loss for the integrated photocurrent intensity under different grain size dispersion.

Finally, we can further present a theoretical estimation of the photocurrent intensity $I_{ph} = \int_{E_g}^\infty \alpha T_{QD} d(\hbar\omega)$ to gain more insight. We use the approximation of rectangular wells with corresponding standard deviation D_R in size in nc-Si films for the calculation of the tunneling coefficient T_{QD} via numerical method [18]. The theoretical results in Fig. 3(c) (solid curve) can basically predict the experimental data, demonstrating that the photocurrent intensity is determined by the photoresponse broadening in small size fluctuation, while the tunneling transport process will overwhelm the increase of optical absorption under large size dispersion condition. As a result, we are able to tune the photoresponse through size distribution control of the Si quantum dots and suitable size dispersion is desirable for the real application of semi-conductor nanomaterials in solar cells to balance the absorption enhancement and tunneling loss.

In summary, we have presented a strategy to maximize the photocurrent intensity through size distribution control of Si quantum dots in nc-Si thin films. Raman mapping technique has been employed to extract the grain size dispersion within the nc-Si thin films. With the aid of the existence of multiple energy states identified from the current–voltage measurements, we are able to decompose the photocurrent spectra, where the photocurrent

characteristics (peak position, linewidth, and intensity) have been well explained by the average dot size and grain size deviation through the quantum confinement effect. Both the enhancement of light harvest via the photoresponse broadening and tunneling loss due to the misalignment of energy levels have been observed in Si quantum dots with increasing size dispersion. In combination with the theoretical calculation for the integrated photocurrent intensity, we have demonstrated the possibility to tune the photoresponse through size distribution control of the Si quantum dots, indicating that suitable size dispersion is desirable for the real application of semiconductor nanomaterials in solar cells.

Acknowledgments

This work was supported by the Natural Science Foundation of China (contract nos. 10734020 and 11074169), National Major Basic Research Project of 2010CB933702, and Shanghai Municipal Commission of Science and Technology Project of 08XD14022.

References

[1] J. Yang, B.J. Yan, S. Guha, Thin Solid Films 48 (2005) 162.
[2] Photovoltaic Technology Research Advisory Council (PV-TRAC), A Vision for Photovoltaic Technology for 2030 and Beyond, European Communities, 2004.
[3] D.L. Staebler, C.R. Wronski, Appl. Phys. Lett. 31 (1977) 292.
[4] R. Zhang, X.Y. Chen, K. Zhang, W.Z. Shen, J. Appl. Phys. 100 (2006) 104310.
[5] Y. Mai, S. Klein, F. Finger, Appl. Phys. Lett. 85 (2004) 2839.
[6] K. Yamamoto, M. Yoshimi, T. Sawada, S. Fukuda, T. Suezaki, M. Ichikawa, Y. Koi, M. Goto, T. Meguro, T. Matsuda, M. Kondo, T. Sasaki, Y. Tawada, Prog. Photovolt.: Res. Appl. 13 (2005) 489.
[7] A. Kongkanand, K. Tvrdy, K. Takechi, M. Kuno, P.V. Kamat, J. Am. Chem. Soc. 130 (2008) 4007.
[8] E.A. Weiss, V.J. Porter, R.C. Chiechi, S.M. Geyer, D.C. Bell, M.G. Bawendi, G.M. Whitesides, J. Am. Chem. Soc. 130 (2008) 83.
[9] K.H. Li, W.Z. Shen, J. Appl. Phys. 106 (2009) 063505.
[10] M. Yang, D.M. Huang, P.H. Hao, F.L. Zhang, X.Y. Hou, X. Wang, J. Appl. Phys. 75 (1994) 651.
[11] Y.T. Dai, J.C. Fan, Y.F. Chen, R.M. Lin, S.C. Lee, H.H. Lin, J. Appl. Phys. 82 (1997) 4489.
[12] R. Zhang, X.Y. Chen, J.J. Lu, W.Z. Shen, J. Appl. Phys. 102 (2007) 123708.
[13] V.V. Nikolaev, N.S. Averkiev, Appl. Phys. Lett. 95 (2009) 263107.
[14] I. Filikhin, S.G. Matinyan, B.K. Schmid, B. Vlahovic, Physica E 42 (2010) 1979.
[15] W.Y. Wu, J.N. Schulman, T.Y. Hsu, U. Efron, Appl. Phys. Lett. 51 (1987) 710.
[16] D.L. Ferreira, J.L.A. Alves, Nanotechnology 15 (2004) 975.
[17] J. Callaway, Quantum Theory of the Solid State, Academic, New York, 1974.
[18] Y. Ando, T. Itoh, J. Appl. Phys. 61 (1987) 1497.